Anal. Bioanal. Electrochem., Vol. 9, No. 3, 2017, 312-327

Analytical & Bioanalytical Electrochemistry

2017 by CEE
www.abechem.com

Full Paper

Synthesis and Electrochemical Characterization of Pr-doped Li-rich Mn-based Layered Oxides $Li[Li_{0.2}Mn_{0.54}Ni_{0.13}Co_{0.13}]O_2$ for Li-ion Batteries

Fatemeh Poursalehi[1, 2] and Mehran Javanbakht[1,2,*]

[1]*Department of Chemistry, Amirkabir University of Technology, Tehran, Iran*
[2]*Renewable Energy Research Center, Amirkabir University Of Technology, Tehran, Iran*

*Corresponding Author, Tel.: +98 21 64545806
E-Mail: mehranjavanbakht@gmail.com

Received: 11 March 2017 / Received in revised form: 8 April 2017 / Accepted: 16 April 2017 / Published online: 15 May 2017

Abstract- Li-rich Mn-based layered oxides, which are considered as solid solutions of $xLi_2MnO_3.(1-x)LiMn_{0.33}Ni_{0.33}Co_{0.33})O_2$ have attracted much attention for their high theoretical capacity (>250 mAh g^{-1}) and operating voltage (>3.5 V *vs.* Li/Li^+). In this research work, synthesis, electrochemical investigation of $Li_{1.2}Mn_{0.54}Ni_{0.13}Co_{0.13}O_2$ and influence of the doping Pr^{3+} ion on its structure and properties has been investigated. These Li-rich cathode materials with the general formula of $Li_{1.2}Mn_{0.54-x}Ni_{0.13}Co_{0.13}Pr_xO_2$ (x=0, 0.01, 0.03, 0.05) have been synthesized by a hydrothermal method. The synthesis of samples and increase of cell volume was confirmed by X-ray diffraction. The stoichiometric ratios for x=0.03 according to experimental formula of $Li_{1.2}Mn_{0.50}Ni_{0.12}Co_{0.13}Pr_{0.02}O_2$ were determined by inductively coupled plasma (ICP) method. In order to better understand the morphology of the synthesized samples, SEM analysis was applied and in order to specify particles distribution, EDS images were prepared. The purpose of this study is achieving better electrochemical properties such as cycle performance. The ability of these materials as a cathode in Li-ion batteries was studied with cyclic voltammetry, Electrochemical Impedance Spectroscopy (EIS) and galvanostatic charge/discharge methods. The doped compound with x=0.03 exhibited the higher columbic efficiency and cycle performance, which delivering an initial discharge capacity of 247 mAh g^{-1} at 0.05 C and 195 mAh g^{-1} after 10 cycles with capacity retention of 79%, compared to pristine sample with capacity retention of 62% retention. The columbic efficiency of the pristine sample was promoted from 79% to 83% for

the doped sample. The results of EIS demonstrated that doping with Pr^{3+} ions reduces the charge transfer resistance from 696 μΩ to 252 μΩ and facilitates the Li ion diffusion.

Keywords- Li-ion battery, Li-rich cathode material, Doping, Rare earth element, Hydrothermal synthesi

1. INTRODUCTION

With the shortage of non-renewable energy sources and the problems such as air pollution, earth heating and greenhouse gas emission, the growing demand for green energy sources becomes very important. Furthermore, in 21st-century tremendous efforts have been made for the development of requirements for energy storage [1,2]. Li-ion batteries have dominated the share of rechargeable batteries market for a variety of applications ranging from hybrid electric vehicles to modern portable electronics due to their high energy density and operating voltage [3,4]. One way to meet L-ion batteries with higher energy density is to find superior cathode materials since they exhibit lower capacity compared to anode materials [5,6].

Over the past decade, Li-rich Mn-based (LMNCO) layered solid solution systems $xLi_2MnO_3.(1-x)LiMO_2$ (M= Mn, Ni, and Co) have been presumed to be promising for their higher specific capacity (>250 mAh g^{-1}), operating voltage (>3/5 V) compared to conventional commercial cathode materials such as $LiFePO_4$, and $LiMn_2O_4$ and also lower cost, higher safety and environmental friendliness compared to $LiCoO_2$ [7-9]. In spite of these facts, the way LMNCO cathode material from laboratory-scale to practical applications has been blocked as they suffer from three serious limitations: (1) low initial columbic efficiency caused by irreversible activation of Li_2MnO_3 component and decrease in the number of Li-ion sites due to elimination of oxide ions vacancies at the end of the first charge, (2) undesirable rate performance, which is related to poor Li^+ diffusion of these cathode materials and low electronic conductivity in conjunction with Mn ions and (3) capacity fade with cycling because of the crystal structural evolution [10].

To overcome the aforementioned drawbacks of cathode material, partial substitution strategy easily progresses electrochemical performance without additional processing steps and costs and has been successfully used so far [11]. There have been many studies on partial substitution at transition metal (TM) sites or cationic doping with Zn^{2+} [12], Mo^{6+} [5], Cr^{3+} [13], and Ti^{3+} [14]. The doped samples showed better discharge capacity, rate capability, columbic efficiency, layer structure ordering, lattice parameters or cycle performance [11]. However, it was found that each dopant only enhanced some particular aspects of electrochemical performance, not all. For example, Zn^{2+} dopants reduced capacity caused by the substitution of inactive for active components and occupied Li-ion sites due to its similar radius of Zn-ions to Li-ions [12,15]. Thus the selection of the doping element is major of significance in improving the electrochemical properties of the LMNCO cathode materials.

Generally, rare earth elements (REEs) are particularly suitable for doping agents, owing to their excellent thermal and chemical stability, high mechanical resistance and low moisture absorption [16]. So far, REEs such as Ru^{3+} [17], Y^{3+} [18], and Sm^{3+} [19] have been used as doping agents in LMNCO cathode materials. According to Long's Handbook of Chemistry, the bond dissociation of the M-O is stronger than Mn-O, which contributes to the stability of the bulk layered structure. Meanwhile, the doped ions expand the Li^+ channel in the layered structure due to their larger radius as compared to the TM ions [16]. Obviously, substituting with REEs is a good method to modify the structural and electrochemical performance of NMC and LMNCO cathode materials [18]. Kang et all replaced Co^{3+} by other low cost and more environment-friendly elements, since cobalt is the most expensive and toxic functional element in LMNCOs [18]. Chen et. all substituted all TM sites, which are difficult to control since several transition metals with different oxidation states coexist in the TM layer [18,20]. We proposed to introduce the REE (Pr) into the $Li[Li_{0.2}Mn_{0.54}Co_{0.13}Ni_{0.13}]O_2$ structure as the replacement at Mn sites with regard to the specific role of transition metal manganese in the LMNCO cathode material [19]. To the best of our knowledge, the influence of Pr^{3+} doping on Li-ion batteries has rarely been reported.

In our previous works other cathode materials were successfully synthesized with different modifications that some of them are explained here. Flower-like lithium iron phosphate with good electrochemical performance was synthesized by a hydrothermal method [21]. A novel binary solvent of ethylene glycol/water medium (W/EG 50:50) was used that plays an important role in the formation of the hierarchical meso-structures of bow-tie-like composition units composed of self-assembly lithium iron phosphate (LFP) nano-sheets [22]. $LiFePO_4$/graphene active material (LFP/G) was successfully synthesized via a simple, low raw material cost and environment friendly hydrothermal method at 170 °C [23]. In the last work, a novel and simple method was reported to prepare high rate performance CuO/graphene nanosheets (GNs) modified LiFePO4 cathode composites (CLFP/G/CuO) via co-precipitation followed by hydrothermal method. Incorporation of CuO into graphene nanosheets greatly enhanced the electrical conductivity and electrochemical performance of the LFP/graphene (LFP/G) cathodes throughout the cycle process [24].

In this work, a series of LMNCO layered oxide materials $Li[Li_{0.2}Mn_{0.54-x}Ni_{0.13}Co_{0.13}Pr_x]O_2$ (x=0, 0.01, 0.03, 0.05) were successfully prepared by a simple hydrothermal reaction. The praseodymium has extraordinary features such as super-large ionic radius (0.99 A°), strongest bond dissociation energy of M-O (753 kJ mol^{-1}) and highest electronic conductivity (with electrical resistance of 70 μΩ) among the REEs dopants used in LMNCO cathode material. The aforementioned features are expected to have an undeniable role to improve columbic efficiency and cycle ability of $Li[Li_{0.2}Mn_{0.54}Ni_{0.13}Co_{0.13}]O_2$ cathode material. The effect of rare earth element Praseodymium doping on the crystal structure, lattice parameters, as well as morphology and electrochemical behavior were carefully

investigated. In addition, the reasons for the improved cycling performance and columbic efficiency were thoroughly discussed.

2. EXPERIMENTAL

2.1. Synthesis of cathode materials

The LMNCO layered oxides $Li[Li_{0.2}Mn_{0.54-x}Ni_{0.13}Co_{0.13}Pr_x]O_2$ (x=0, 0.01, 0.03, 0.05) were prepared by a simple hydrothermal method. All the chemical reagents (Sigma-Aldrich) were of commercially available analytical grade and were used without further purification. The starting material were lithium acetate ($LiCH_3COO.2H_2O$), Manganese(II) acetate ($Mn(CH_3COO)_2.4H_2O$), nickel(II) acetate ($Ni(CH_3COO)_2.4H_2O$), cobalt(II) acetate ($Co(CH_3COO)_2.4H_2O$), and praseodymium nitrate ($Pr(NO_3)_3.6H_2O$) used in 1.2: 0.54-x: 0.13: 0.13: x molar ratio with initial concentration of 1.5, 0.67, 0.2, 0.2 and 0.2 mol L^{-1}, respectively. The reagents were dissolved in a mixture solvent of water, 2-propanol, and acetonitrile with the volume ratio of 1: 1: 1 (except for Pr just in water solvent) to form a transparent and homogeneous solution. The mixed solution of nickel and cobalt was added to the mixed solution of lithium and manganese under stirring to form the final mixture. For the doped samples, the solution of praseodymium was added to manganese solution firstly.

1 M solution of Oxalate ($H_2C_2O_4$, Sigma-Aldrich, 99% purity) was added to the above final mixture drop wisely under magnetic stirring as both complexing agent and precipitant until the solution turned to be slurry-like. After stirring for 60 min, the homogenous slurry was transferred and sealed in a 50 ml poly tetrafluoroethylene (Teflon)-lined stainless steel reactor with the volume filling ratio of >50%.

The autoclave was immersed in a silicon oil bath followed by continuously heating and stirring on the hot plate magnetic stirrer at the temperature of 160 °C for 24 h with 500 rpm rate and then cooled down to room temperature naturally. After the reaction, the autoclave was discharged and the pink precipitate was gathered with centrifuging and then washed with deionized water several times, followed by drying at 80 °C in a vacuum oven for some hours to obtain the precursor. In order to compensate for the loss of Li at the high reaction temperature, the dried powder was mixed thoroughly with approximate additional lithium acetate (precursor: $LiCH_3COO$=1: 0.2 by weight ratio). After grinding, the mixed powder was annealed in the air by a three-step heating program, first preheated at 250 °C for 2 h, then decomposed at 500 °C for 6 h, and finally calcined at 650 °C for 6 h. The final materials were obtained by cooling them to room temperature in the furnace.

The LMNCO layered oxide $Li[Li_{0.2}Mn_{0.54-x}Ni_{0.13}Co_{0.13}Pr_x]O_2$ (x=0, 0.01, 0.03, 0.05) samples were labeled Pr-0, Pr-1, Pr-2 and Pr-3 for Pr molar ratio of x=0, x=0.1, x=0.03 and x=0.05, respectively.

2.2. Characterization

The phase identifications and crystallinity of synthesized powders were conducted with X-ray diffraction (XRD, EQuniox 3000, Intel FRANCE) using Cu Kα radiation between 5° and 110° (2θ degree) at a step size of 3° min^{-1} for analyzing (λ=0.15418 nm). The morphology of the powders was observed with scanning electron spectroscopy (SEM, VEGA-XMU, TESCAN), equipped with energy dispersive X-ray spectroscopy (EDX) analysis, which was conducted to test the elemental distribution on the surface of the cathode material. The relative amounts of Li, Mn, Ni, Co, and Pr in the samples were monitored by conducting inductively coupled plasma-atomic emission spectroscopy (ICP-AES, VISTA-PRO, VARIAN Australia).

2.3. Electrochemical measurement

For the electrochemical test, the samples electrode were fabricated contains on a dry basis 85%wt the $Li_{1.2}Mn_{0.54}Ni_{0.13}Co_{0.13}O_2$ powder either with or without Pr doped, 10% ultrapure graphite (purity>99.99 wt.%) and 5 wt% PVDF (poly vinylidene fluorides, as a binder) in NMP (N-methyl 2-pyrollidine, as a solvent). The mixed slurry was coated onto an Al foil and then dried in vacuum oven for 6 h in 80 $^{\circ}$C to evaporate the solvent. Metallic lithium foil was used as the anode electrode; 1 M $LiClO_4$ (battery grade, Sigma-Aldrich) in propylene carbonate (PC) as the electrolyte. The micro-pores polypropylene membrane (Celgard 2400) was used to separate the working electrode and a lithium foil counter electrode. The coin-cells were assembled in an Argon-filled glove box. The galvanostatic charge/discharge measurements were carried out in the voltage range of 2–4.8 V (versus Li/Li^+) using a battery tester (Kimiastat-5 V/10 mA, Kimia pardaz rayane, Iran) with current density of 0.05 C for many cycles.

Cyclic voltammetry (CV) was measured by an electrochemical working station at a scan rate of 0.1 mVs^{-1} between 2-4.8 V (versus Li/Li^+). Electrochemical impedance spectroscopy (EIS) was conducted also on the same electrochemical working station with an AC oscillation of 5 mV amplitude over the frequencies between 100 KHz to 10 mHz. The EIS spectra are fitted with an equivalent circuit as shown in the inset image. The CV and EIS measurement were carried out using Galvanostat/Potentiostat Autolab (PGSTAT 302N). All the electrochemical measurements were carried out at room temperature (25 °C).

3. RESULTS AND DISCUSSION

3.1. Structure, composition and morphology

The XRD patterns of $Li[Li_{0.2}Mn_{0.54-x}Ni_{0.13}Co_{0.13}Pr_x]O_2$ (x=0, 0.01, 0.03, 0.05) are shown in Fig. 1. The I(003)/I(104) for all samples is illustrated in Table 1. Herein the

$Li_{1.2}Mn_{0.54}Ni_{0.13}Co_{0.13}O_2$ cathode material, which is written in form of $0.55Li_2MnO_3.0.45LiMn_{0.33}Ni_{0.133}Co_{0.33}$ is considered as a composite form with two integrated layered structures of $LiMO_2$ alternated with Li_2MnO_3 layer [9].

Several weak super lattice reflection peaks between 20° and 25° are related to Li_2MnO_3 monoclinic component (with space group of C2 / m), which are compatible with cation array of $LiMn_6$ (or local phase $LiMn_{6-x}M_x$ (M=Mn, Ni, Co) in TM layers that usually exist in unit cells of Li_2MnO_3 ($Li(Li_{1/3}Mn_{2/3})$). This regular arrangement is due to the electronic intercalation and charge ordering among Co, Mn and Ni ions. In a simple way, it could be said super lattice peaks are related to present presence of Li^+ and Mn^{4+} ions in TM layer. All the remained reflection peaks are indexed to the hexagonal layered $LiMO_2$ component of a α-NaFeO2 type (with space group pf R3m) [17, 25, 26].

Similar patterns of doped and pristine samples and lack of existence of impurity phase indicate that the Pr-doped samples retain the single phase of unsubstituted $Li_{1.2}Mn_{0.54}Ni_{0.13}Co_{0.13}O_2$ and partial substitution of Mn with Pr is achieved successfully. Indeed, a small substituting ratio is located in the lattice crystal sites and leads to high purity of oxide layers [18, 22]. However, by increasing the dopant to the high level of x=0.05, distinct peaks emerge, which are indexed as Pr_2O_3 phase (PDF#01-078-0309). These impurities, which are originated from excess praseodymium doping, lead to higher inferior crystallinity [18].

Another observation in XRD patterns is the sharp peaks and clear separation of the (006)/(012) and (018)/(110) peaks, which indicates the formation of a well-crystallized layered structure in all samples [22]. On the other hand, the intensity ratio (003)/(104) diffraction peaks can directly indicate cation mixing of $Li(Ni_{1/3}Co_{1/3}Mn_{1/3})O_2$, which has a great effect on the electrochemical performance of the cathode materials [16]. A value of <1.2 indicates a high degree of cation mixing in the lattice, primarily due to the similar radius of Mn^{4+} (0.53A°), Ni^{2+} (0.69 A°), Co^{3+} (0.68 A°) and Li^+ (0.76 A°), which deteriorate the electrochemical performance [23]. It is seen in Table 1 that the values of the I(003)/I(104) ratios are greater than 1.2 and also increase greatly after doping, which shows the low ion mixing in the doped samples due to the distinct radius of Pr^{3+} (0.99 A°) to the bulk ions [17,19]. Table1 demonstrates that the sample Pr-2 (with x=0.03) shows the highest I(003)/I(104) ratio, indicating that the sample formed a pure phase with high crystallinity and low cation mixing and this means that a good electrochemical performance of this material can be expected [18,27].

The diffraction peaks of the doped materials slightly shift to lower 2θ as compared to that of the undoped material as shown in Fig. 1, which indicates that Pr-doped samples have larger lattice constants and cell volume than the pristine [18,27]. This may be due to the larger radius of the Pr^{3+} (0.99 A°) than that of Mn^{4+} (0.54 A°) [15] and could provide more lattice space for Li^+ intercalation/deintercalation and prevent the structure from breaking [12].

According to results from the first principle calculation from Ceder's group, the activation energy of Li diffusion from original octahedral sites to interslab tetrahedral sites is strongly dependent on the distance between oxygen layers. The energetic barrier of hindering Li diffusion could be weakened apparently by the increase in Li slab distance, thereafter, improves the ability of Li diffusion upon charge and discharge. Hence, it is expected that the electrochemical performance, especially cycle ability, can be enhanced due to Pr doping [17].

Table 1. Comparison of pristine and Pr-doped sample powders

Sample	I(003)/I(104)
Pr-0	1.36
Pr-1	1.58
Pr-2	1.63
Pr-3	1.27

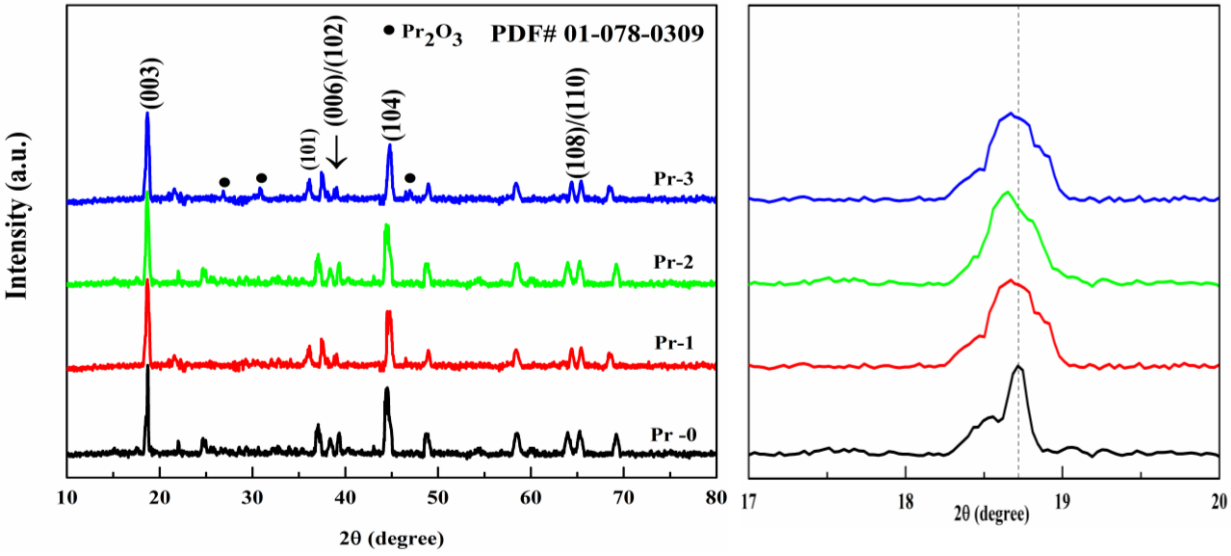

Fig. 1. XRD patterns of Pr-0, Pr-1, Pr-2, Pr-3 and the magnified view of peak (003)

Fig. 2 shows the SEM images of pristine and Pr-doped samples. All the powders have a similar uniform morphology of cubic particles with high homogeneity. Moreover, agglomeration of the particles, which is observed in the structure, is due to the small particle size of synthesized samples. The morphology of samples has not changed clearly with the increase of Pr content.

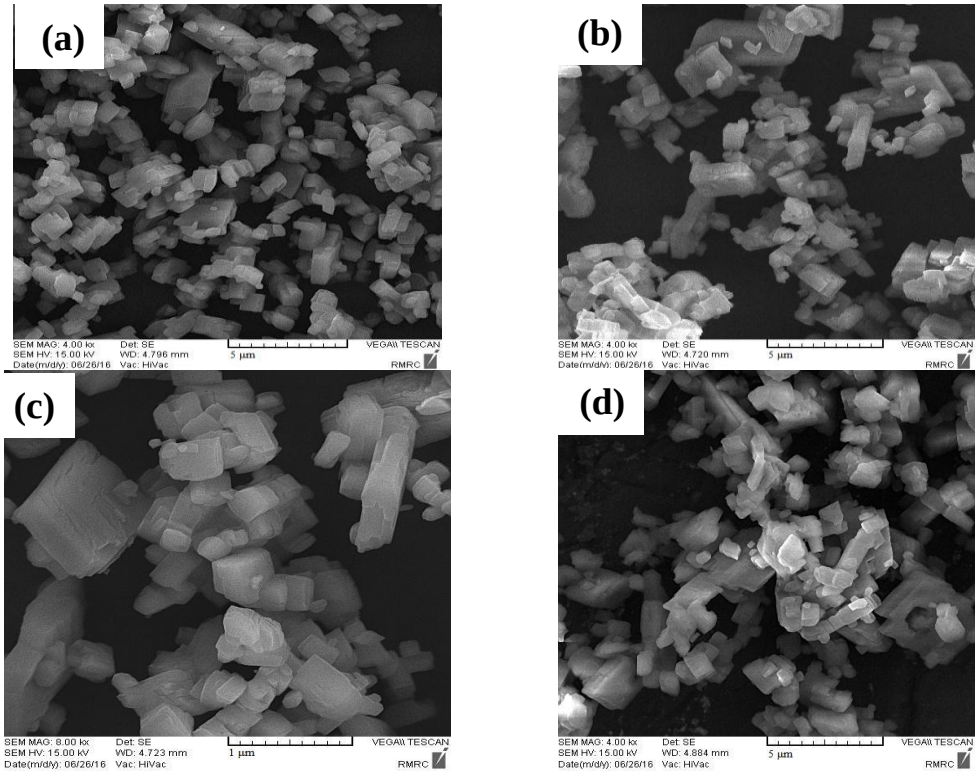

Fig. 2. SEM images of the prepared pristine and Pr-doped samples: (a) Pr-0, (b) Pr-1, (c) Pr-2 and (d) Pr-3

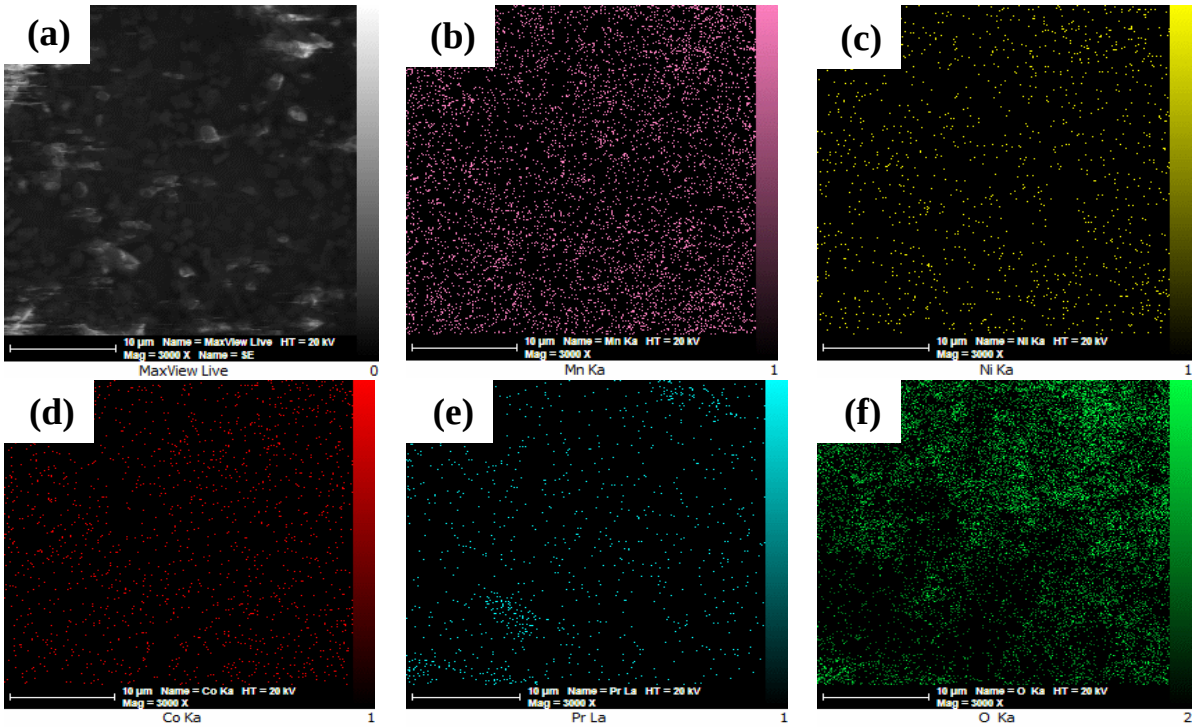

Fig. 3. The elemental mapping of the prepared Pr-2 sample, (a) Pr-2, (b) Mn, (c) Ni, (d) Co, (e) Pr and (f) O by scanning transmission electron microscope

The elemental distributions on the surface of $Li[Li_{0.2}Mn_{0.51}Ni_{0.13}Co_{0.13}Pr_{0.03}]O_2$ are monitored by energy-dispersive X-ray spectroscopy and are shown in Fig. 3. There is no segregation for the doped materials, which confirms that the Pr elements are distributed in the sample homogenously. It is concluded from XRD analysis and EDS images that rare earth element Pr has doped into the $Li[Li_{0.2}Mn_{0.54}Ni_{0.13}Co_{0.13}]O_2$ structure successfully.

The quantities of the chemical composition of Pr-2 are presented in Table 2 and confirm that the relative amounts of as-synthesized material are in agreement with the designed one. The relative high Li amounts are probably because of the excess CH_3COOLi in the calcination process.

Table 2. Relative contents of Li, Mn, Ni, Co and Pr in the Pr-2 sample

samples	Li	Mn	Ni	Co	Pr
Theoretical sample	1.20	0.51	0.13	0.13	0.03
Experimental sample	1.23	0.50	0.12	0.13	0.02

3.2. Electrochemical properties

Fig. 4 shows the initial charge and discharge curves of sample Pr-0 and Pr-2. The charge-discharge process was operated over the potential range of 2-4.8 V at 0.05 C. The initial charge and discharge capacities and the initial columbic efficiency of electrodes before and after modification are listed in Table 3. The initial charge capacity of Pr-2 sample is 301 $mAhg^{-1}$, which is lower than pristine sample (340 $mAhg^{-1}$). The decrease of capacity can be attributed to strong Pr-O bond. Comparing to Mn-O bond, the formation of stronger Pr-O bond can suppress the extraction of Li^+ and O^{2-} from Li_2MnO_3 component during the initial charge process [12]. In other words, Pr doping helps inhibit the release of O from the structure and the initial charge capacity decreases quickly because of the depressed oxygen from the crystal lattice.

Table 3. The initial charge-discharge capacities and efficiencies of the Pr-0 and Pr-2 electrodes

Sample	Charge capacity (mAh g^{-1})	Discharge capacity (mAh g^{-1})	Initial efficiency
Pr-0	340	268	79%
Pr-2	301	247	83%

Also, the discharge capacity of doped sample is a little lower than pristine since a portion of the initial discharge capacity of LMNCO cathode originates in the reversibility of lattice oxygen [19]. But the low initial efficiency of Li-rich solid solution of pristine cathode has been improved when doped with rare earth element Pr, which is related to suppression of irreversible activation of Li_2MnO_3 component [12].

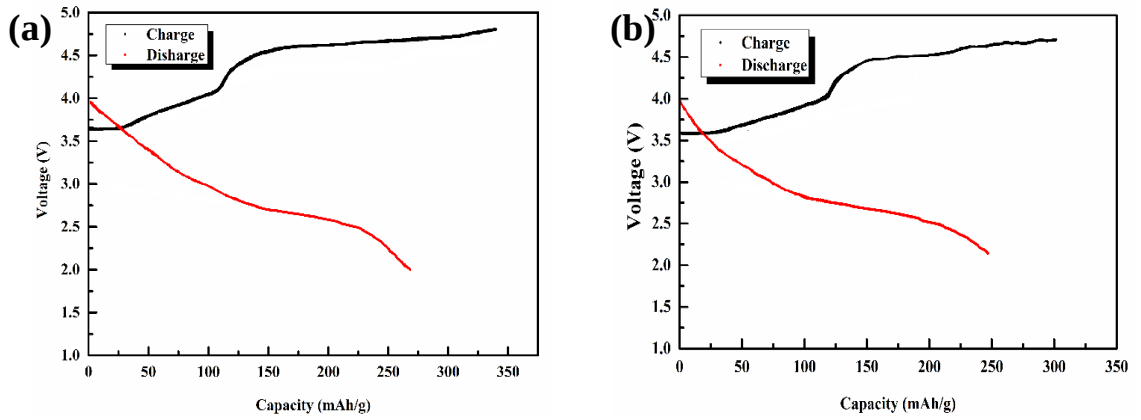

Fig. 4. Initial charge and discharge curves of (a) Pr-0 and (b) Pr-2 at current density of 0.05C over the voltage range of 2-4.8 V

In order to compare cycle ability of the doped and pristine sample, the recycling capacities of Pr-0 and Pr-2 samples, which were charged and discharged between 2.0 V and 4.8 V are presented in Fig. 5. This figure shows discharge capacity versus cycle number. The Pr-2 electrode delivers 195 $mAhg^{-1}$ after 10 cycles and the capacity retention ratio is 79%, while only 165 mAh g^{-1} and 62% are obtained after 10 times of cycling for the pristine electrode. These data indicate that an appropriate amount of Pr dopant in the sample can enhance the cycling performance. The reason for the enhanced cycling performance of the Pr-doped materials may be found from the change of lattice parameter caused by Pr doping. After doping the sample, the cell volume V increase, which will make a larger Li^+ path during the Li^+ intercalation and deintercalation..

Table. 4. Cycling performance of Pr-0 and Pr-2 samples at the current density of 0.05C

Sample	Initial discharge capacity (mAh g^{-1})	Second discharge capacity (mAh g^{-1})	cycle number	Capacity retention
Pr-0	268	165	10	62%
Pr-2	247	195	10	79%

So Li^+ intercalation will be easier during charge-discharge process, and it act as a supporting pillar and minimize the structure constriction, which eventually would lead to better cycling ability in the Pr-doped materials compared with the undoped one [20]. Since Pr-O possesses much higher bonding energy (753 kJ mol^{-1}) than Mn-O (402 kJ mol^{-1}), the Pr-doping can stabilize the crystal structure of cathode material by suppression of layered-to-spinel phase transformation [16,18]. As a result, the electrochemical performance of cathode has been enhanced

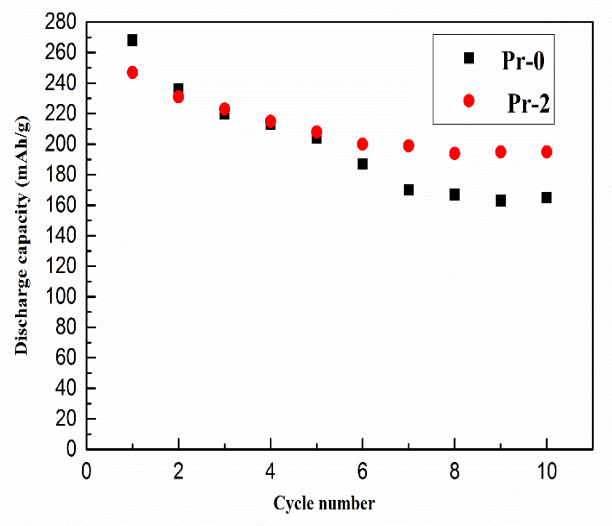

Fig. 5. Discharge capacities *vs.* cycle number of coin-type cells composed of pristine and Pr-doped LMNCO cathode (a) Pr-0, (b) Pr-2 and a Li metal anode. Test cells were cycled as galvanostatic between 2 and 4.8 V versus Li^+/Li at 0.05C rate

Cyclic voltammetry of Pr-0 and Pr-2 was conducted to evaluate the redox potential of the transition metal ions during cycling at scan rate of 0.1 mV s^{-1} between 2 and 4.8 V (versus Li^+/Li). Cyclic voltammetry traces of first cycle are shown in Fig 6. The first anodic peak at approximately 4.0 V is associated with the oxidation of Ni^{2+} to Ni^{3+}/Ni^{4+} and the second anodic peak at a higher potential (around 4.5 V) is associated with the irreversible electrochemical activation reaction that strips Li_2O from Li_2MnO_3 component. The intensity of oxidation peak at 4.5 V of Pr doped electrode decreases in comparison with the pristine electrode, which shows the release of oxygen has been restrained because of the presence of Pr in the initial charging process [19]. At the end of the first charge process, Mn ions remain at the tetravalent. During the first discharge the weak peak at 3.3V is due to the reduction of Mn from tetravalent to a certain state above trivalent [17]. Indeed, the peak at 3.3 V in the initial cycle for the pristine electrode refers to the reduction of activated Mn^{4+} to Mn^{3+}. The reduction peak at 3.3 V, which has disappeared in the Pr doped samples, indicates the doping

of Pr inhibits the activation of element manganese, which would restrain the dissolution of manganese in the subsequent cycles, and the stability of crystal structure is assured [19].

The overlapping degree is different between Pr-0 and Pr-2 samples, which are related to large electrochemical polarization and decay of discharge plateau. The electrochemical reversibility can be characterized by the voltage difference (ΔE_p) between the anodic and cathodic peak. The ΔE_p of Pr-0 and Pr-2 are 0.48 V and 0.28 V, respectively. Pr-2 sample exhibiting smaller ΔE_p implies that the layered structure of $Li[Li_{0.2}Mn_{0.54}Ni_{0.13}Co_{0.13}]O_2$ cathode materials could be stabilized and the polarization could be restrained by moderate Pr doping.

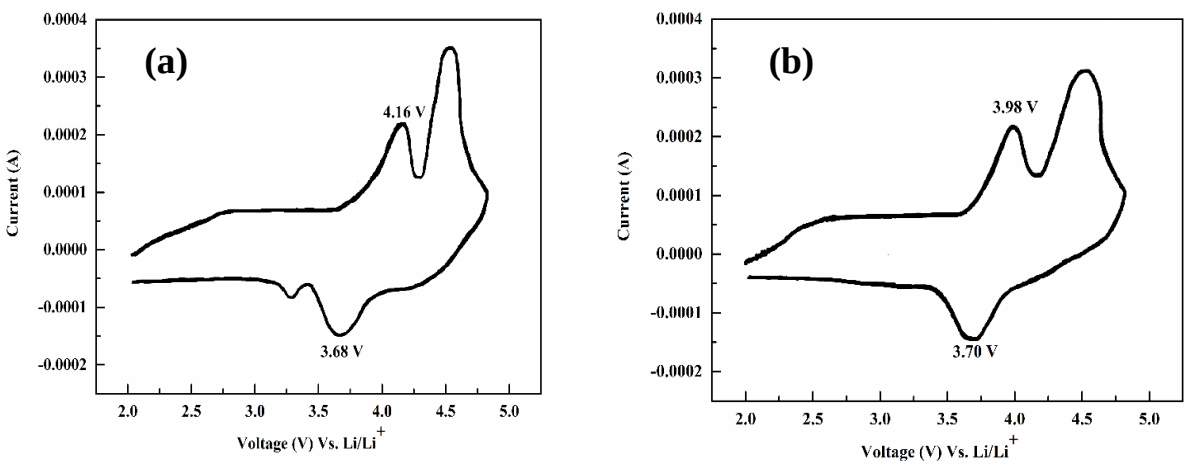

Fig. 6. Cyclic voltammograms of (a) Pr-0 and (b) Pr-2 electrodes for the first cycle. CVs were recorded at the voltage range of 2-4.8 V at a scan rate of 0.1 mV s^{-1}

To further understand the effects of Pr^{3+} in the layered structure on the electrochemical properties of the Pr-2 doped material, EIS measurement was carried out to explore the kinetic parameters of Li^+ intercalation/deintercalation between the pristine and Pr-2 doped materials. The obtained plots, as shown in Fig. 7 consist of a depressed semicircle in high frequency region and sloping line in low frequency region (Z' is the real impedance and Z'' is the imaginary impedance). The semicircle is related to charge transfer resistance (R_{ct}) at the interface of cathode and electrolyte while the sloping line is related to Warburg impedance, which is attributed to the solid-state diffusion of Li^+ into the active electrode. To further identify the electrochemical properties of the two samples, the equivalent circuit model corresponding to Fig. 7 is set up by Nova fitting software. In the equivalent circuit, R_s and R_{ct} show the solution and charge transfer resistance, respectively, CPE_{ct} is the constant charge transfer capacitance of the layer electrode material, and Z_w is the Warburg impedance for lithium ion diffusion in the bulk material [5]. The parameters of the equivalent circuit calculated from equivalent circuits are all listed in Table 5. The quantity of R_s in both samples is low and near each other because of the same electrolyte in each test. The small

difference in resistance of electrolyte is attributed to errors in preparing electrolyte such as drying solvents, weighting lithium perchlorate, moisture of laboratory dishes and etc. The R_{ct} in Pr-2 cathode materials is 252 Ω. The Pr-2 sample has the smaller R_{ct} than pristine sample $Li[Li_{0.2}Mn_{0.54}Ni_{0.13}Co_{0.13}]O_2$ (696 Ω) because of the improved electronic conductivity, which indicates the consequent improvement in high-rate capabilities and an enhancement in the kinetics [5]. On the other hand, it can be attributed to the expansion of lattice crystal, which promotes the process of Li^+ intercalation/deintercalation. This may be explained by the enlarged lattice volume of Pr^{3+} doped samples, which indeed favors the Li^+ diffusion [12,27]. In addition, the exchange current densities (i_0) of samples are calculated by the formula (i_0=RT/nFR_{ct}, where n is the number of transferred electrons) and are listed in Table 5. The Pr-doped material shows higher exchange current density (1.02×10^{-4} $mAcm^{-2}$) compared to pristine material (3.68×10-5 $mAcm^{-2}$) [20].

Table 5. Impedance parameters of Pr-0 and Pr-2 electrodes

Sample	R_s (Ω)	R_{ct} (Ω)	C_{dl} (μF)	I_0 (mA cm^{-2})
Pr-0	7.26	696	73.21	3.68×10^{-5}
Pr-2	9.08	251	26.72	1.02×10^{-4}

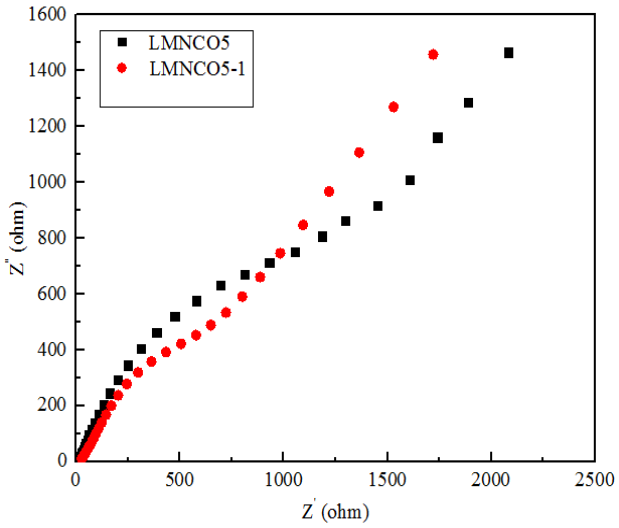

Fig. 7. Electrochemical impedance spectra of Pr-0 and Pr-2 electrodes measured in the frequency range between 100 KHz and 10 mHz. Inset is the corresponding equivalent circuit used for simulating the plot fitting

The high value of CPE_{ct} means high constant charge transfer capacitance of the layer electrode material, which results in serious capacity fading at high rates, while Pr-2 show low CPE_{ct} value. Therefore, it can be concluded that the improvement of the Li^+ ion diffusion in SEI and the electrochemical reaction activity are responsible for the better cycling ability and

rate capability of the doped material as well. It may be due to the less severe cathode degradation after doping during the cycling. Hence, the improved initial columbic efficiency and cycle performance of Pr-doped samples can be attributed to the higher Li+ transfer kinetics and the lower charge transfer resistance [18].

Based on the above results, it can be conceded that doping $Li[Li_{0.2}Mn_{0.54}Ni_{0.13}Co_{0.13}]O_2$ with a suitable amount of Pr results in a potentially useful cathode material with low charge transfer and high lithium ion diffusion coefficient.

Table 5 shows the comparison of recent studies on cation doping in LMNCO cathode materials. It is considered from results that the recent research on cation doping with rare earth element Pr is compatible with other studies. It should be noticed that the low cycle number is attributed to the simple synthesis process, which is extensible for industry application.

Table 6. Comparison of recent studies on cationic doping in LMNCO cathode materials

Doped ion	**Element replaced**	**Optimum x amount**	**Discharge capacity (mAh g^{-1}) at 0.05C rate**	**Cycle number**	**Capacity retention**	**Charge transfer resistance (Ω)**	**Published year**	**Ref.**
Sm^{3+}	Mn	0.03	287	40	82%	86	2016	[19]
Sn^{4+}	Mn, Ni, Co	0.01	268	50	96%	200	2015	[28]
Cr^{3+}	Mn, Ni, Co	0.04	243	50	93%	88	2014	[13]
Pr^{3+}	Mn	0.03	247	10	79%	251	2017	This work

4. CONCLUSION

The pristine and Pr-doped $Li[Li_{0.2}Mn_{0.54-x}Ni_{0.13}Co_{0.13}Pr_x]O_2$ (x=0, 0.01, 0.03, 0.05) materials have been synthesized by a simple hydrothermal method. The effect of Pr doping on structure, morphology and electrochemical performance have been studied. Electrochemical data reveals that Pr doping improves the cyclic performance remarkably. The EIS measurements show that Pr doping decreases the charge-transfer resistance and improves the exchange current density. The enhanced electrochemical performances could be related to the improvements in structural stability and conductivity in active electrode by Pr doping.

Acknowledgments

The authors are grateful to the Renewable Energy Research Center (RERC) (Amirkabir University of Technology, Tehran, Iran) for the financial support of this work.

REFERENCES

[1] M. Hu, X. Pang, and Z. Zhou, J. Power Sources 237 (2013) 229.

[2] B. Xu, D. Qian, Z. Wang, and Y. Sh. Meng, Mater. Sci. Eng. 73 (2012) 51

[3] P. Kurzweil, and K. Brandt, Secondary batteries– Lithium, Rechargeable systems, Reference Module in Chemistry, Molecular Sciences and Chemical Engineering, Elsevier, Amsterdam (2009) pp. 1-26.

[4] J. W. Fergu, J. Power Sources 195 (2010) 939.

[5] Y. Zang, C.X. Ding, X.C. Wang, Z.Y. Wen, and C.H. Chen, Electrochim. Acta 168 (2015) 234.

[6] F. He, X. Wang, C. Du, A. P. Baker, J. Wu, and X. Zhang, Electrochim. Acta 153 (2015) 484.

[7] S. N. Lim, J. Y. Seo, D. S. Jung, W. Ahn, H. S. Song, S. H. Yeon, and S. B. Park, J. Alloy Compd. 623 (2015) 55.

[8] D. Ye, K. Ozawa, B. Wang, D. H, Jurcakova, J. Zou, C. Sun, and L. Wang, Nano Energy commun. (2014) 1-10.

[9] J. Wu, H. Liu, X. Ye, J. Xia, Y. Lu, C. Lin, and X. Yu, J. Alloy. Compd. 644 (2015) 223.

[10] J. Yan, X. Liu, and B. Li, RSC. Adv. 4 (2014) 63288.

[11] S. N. Lim, J. Y. Seo, D. S. Jung, S. B. Park, and S. H. Yeon, J. Electroanal. Chem. 740 (2015) 88.

[12] J. Zhao, Z. Wangn, H. Guo, X. Li, Z. He, and T. Li, Ceram. Int. 41 (2015) 11396.

[13] Z. He, Z. Wang, L. Cheng, Z. Zhu, T. Li, L. Li, and H. Guo, Adv. Powder Technol. 25 (2014) 647.

[14] Z. Q. Deng, and A. Manthiram, J. Phys. Chem. A 115 (2011) 7097.

[15] J. Ma, B. Li, L. An, H. Wei, X. Wang, P. Yu, and D. Xia, J. Power Sources 277 (2015) 393.

[16] X. Li, H. Xin, Y. Liu, D. Li, Y. Xu, and X. Qin, RSC Adv. 5 (2015) 45351.

[17] B. Song, M. Lai, and L. Lu, Electrochim. Acta 80 (2015) 187.

[18] S. Kang, H. Qin, Y. Fang, X. Li, and Y. Wang, Electrochim. Acta 144 (2014) 22.

[19] G. Xu, L. J. Xue, Z. Li, X. Li, T. Yu, J. Li, X. Wang, and F, Kang, Solid State Ionics 293 (2016) 7.

[20] H. Chen, Q. Hun, Z. Huang, Z. He, Z. Wang, H. Guo, and X. Li, Ceram. Int. 42 (2016) 263.

[21] M. R. Deylami, M. Javanbakht, M. Ghaemi, and H. Ghafarian, Anal. Bioanal. Electrochem. 5 (2013) 506.

[22] H. Gh. Zahmatkesh, M. Javanbakht, and M. Ghaemi, J. Power Sources 284 (2015) 339.

[23] F. Fathollahi, M. Javanbakht, H. Omidvar, and M. Ghaemi, J. Alloy Compd. 627 (2015) 146.

[24] F. Fathollahi, M. Javanbakht, H. Omidvar, and M. Ghaemi, J. Alloy Compd. 643 (2015) 40.
[25] X. Miao, Y. Yan, C. Wang, L. Cui, J. Fang, and G Yang, J. Power Sources 247 (2014) 219.
[26] F. Wu, Z. Wang, Y. Su, Y. Guan, Y. Jin, N, Yan, J. Tian, L. Bao, and S. Chen. J. Power Sources 267 (2016) 337.
[27] Y. Zeng, K. Qiu, Z. Yang, F. Zhou, L. Xia, and Y. Bu, Ceram. Int. 42 (2016) 10433.
[28] Y. Zhao, M. Xia, X. Hu, Z. Zhao, Y. Wang, and Z. Lv, Electrochim. Acta 174 (2015) 1167.

Copyright © 2017 by CEE (Center of Excellence in Electrochemistry)

ANALYTICAL & BIOANALYTICAL ELECTROCHEMISTRY (http://www.abechem.com**)**

Reproduction is permitted for noncommercial purposes.